Flight Guidance Simulation Employing Non-Linear Dynamic Inversion

A PROJECT
SUBMITTED TO THE FACULTY OF THE GRADUATE SCHOOL
OF THE UNIVERSITY OF MINNESOTA
BY

CHRISTOPHER DANIEL REGAN

IN PARTIAL FULFILLMENT OF THE REQUIREMENTS
FOR THE DEGREE OF
MASTER OF SCIENCE

August 2003

UNIVERSITY OF MINNESOTA

This is to certify that I have examined this copy of a master's project by

CHRISTOPHER DANIEL REGAN

and have found that it is complete and satisfactory in all respects,
and that any and all revisions required by the final
examining committee have been made.

_____

Name of Faculty Adviser(s)

_____

Signature of Faculty Adviser(s)

_____

Date

GRADUATE SCHOOL

Table of Contents

Abstract

An aircraft flight guidance simulator has been developed using a dynamic inversion scheme to control short-period dynamics. This simulation has been developed as a simple means to generate data history for integration into an Inertial Navigation System simulation. Aircraft altitude and heading are controlled by specifying a series of waypoints in a spherical earth based reference frame. The control scheme is shown to be valid across a wide variety of aircraft; from general aviation to commercial airliners.

List of Figures and Tables

Nomenclature and List of Variables

Symbol	Unit	Description
Mach	-	mach number
W	lbs	weight
I_x, I_y, I_z, I_{xz}	slug-in^2	moments of inertia
x_b, y_b, z_b	ft	body frame axes
N, E, D	ft	NED frame axes
u, v, w	ft/s	body fame velocity
X, Y, Z	lbs	body frame forces
L, M, N	ft-lbs	body frame moments
$\dot{N}, \dot{E}, \dot{D}$	ft/s	NED frame velocity
ψ, θ, ϕ	deg	Euler angles (heading, attitude, bank)
Λ, λ, h	deg, ft	Geodetic coordinates
$\dot{\Lambda}, \dot{\lambda}, \dot{h}$	deg/s, ft/s	Geodetic velocity
γ	deg	flight path angle
α	deg	angle of attack
β	deg	sideslip angle
p, q, r	deg/s	body frame rotation rates (yaw, pitch, roll)
$\vec{U}$	-	generic control vector
$\vec{x}$	-	generic states vector
δ_r, δ_e, δ_a	deg	control surface deflections
rng_{alt}	ft	range control parameter
ω_n	rad/s	natural frequency
ζ	-	damping ratio
τ	s	time constant
V_p	ft	vector from center of earth to previous waypoint
V_n	ft	vector from center of earth to next waypoint
V_c	ft	vector from center of earth to current position

$\hat{n}$	-	great circle plane normal unit vector
e	ft	cross-track error
$\dot{e}$	ft/s	cross-track error rate
$\ddot{e}$	ft/s^2	cross-track error acceleration
$\delta\psi$	deg	heading error
$\Delta\psi$	deg	heading change between path legs
m	slug	mass
b	ft	wing span
c	ft	average wing cord
Q	lbs/ft^2	dynamic pressure at nominal velocity
S	ft^2	wing span

Notes:

Subscript “s” denotes a desired or set condition.

Subscript “0” denotes a nominal condition.

Prefix “Δ” denotes a perturbation from nominal.

1 Introduction

1.1 Objective

The purpose of this project was to develop a simple means of generating realistic input data sets for a previously developed Inertial Navigation System (INS) simulation. The data of interest contains details of the aircraft velocity and rotation rate relative to an inertial frame. It was also desirable to develop a means of creating data sets for a diverse set of aircraft.

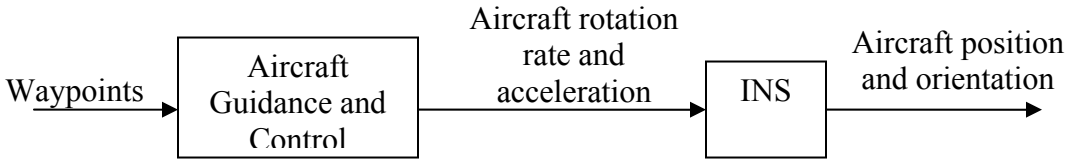

Figure 1.1: Block diagram depiction of guidance system and INS interlink.

1.2 Background

INS systems employ an assembly of sensors to measure, directly or indirectly, the rotation rate and acceleration of an aircraft. The sensors generally consist of three accelerometers and three rate gyros mounted orthogonally. Integrating the rotation rate and acceleration from the sensors yield orientation and velocity. Integrating the velocity again yields the aircraft position. A similar process was used in this project to track aircraft orientation and position.

Several key differences exist between an INS system and the aircraft tracking that has been used in this project. Here all errors that would be associated with sensors are nonexistent. Also, because the sensors of the INS systems are mounted in a moving aircraft, the integration of the sensor values relies on formulating the equations of motion in a true inertial system. For this project the rotation of the earth has been ignored.

1.3 Method

Generating the required data sets could be accomplished by integrating the kinematic equations of motion. This ignores the true dynamic nature of aircraft motion. To capture the dynamics of aircraft motion an aircraft guidance of control simulation has been developed in a Matlab/Simulink environment. Aircraft control has been separated into a set of nested loops. The outer-loop controls the orientation of the aircraft in order to follow a specific trajectory. The inner-loop controls the aerodynamic control surfaces of the aircraft in order to achieve the desired orientation. The basis of the loop separation is based on the assumption that the inner-loop dynamics are much faster than the outer-loop dynamics. Thus the desired path of the aircraft can be achieved without directly addressing the control surface deflections. This is known as "time scale separation", [4].

The inner-loop control is based on non-linear dynamic inversion [4] [5] [6]. This will allow a diverse set of aircraft to be controlled by similar control gains and achieve similar response characteristics. The outer-loop control implements a waypoint based navigation and guidance system; again, diverse aircraft can achieve similar responses.

2 Flight Mechanics

An understanding of the dynamics and kinematics of aircraft is essential to the development of a control law. This section is devoted to the development of the required equations of motion and follows closely the approaches set forth in [1] and [2]. Although the scope of the project was limited to conventional aircraft configurations the derivation of the equations of motion is similar for diverse aircraft.

2.1 Frames, Axis, and Notation

Several reference frames are directly employed to develop the equations of motion. An earth tangent reference (*NED*) frame is employed as well as a body fixed reference (*xyz*) frame in order to describe the orientation of the aircraft. Although traditionally the *NED* reference frame is attached to the surface of the earth, for this project both reference frames originate at the center of gravity of the aircraft. The *NED* frame has the *N* axis directed North, the *E* axis directed East, and the *D* axis points toward the center of earth. The *xyz* body frame has x_b pointing in the aircraft forward direction, y_b points to the right or starboard side of the aircraft, and z_b points down. The orientation of the aircraft is described by relating the xyz frame to the *NED* frame. This is accomplished through a series of rotations defined by the Euler angles (ψ,θ,ϕ). Euler angles are discussed further in Section 2.2.

Forces acting on the aircraft are highly dependent upon the local airflow. The airflow is related to the *xyz* frame by two angles and the aircraft's velocity can also be defined by the same two angles. The angle of attack (α) describes the angle between the body forward direction (x_b) and the relative airflow in the x_b-z_b plane. The flight path angle (γ) describes the angle between the relative airflow in the x_b-z_b plane and the North-East earth plane. Similarly, the sideslip angle (β) defines the angle between the body forward direction (x_b) and the relative airflow in the x_b-y_b plane.

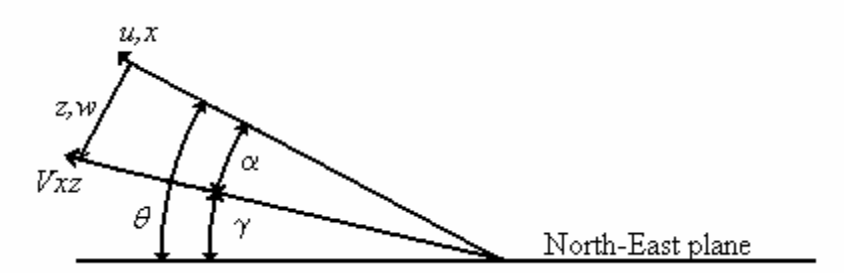

Figure 2.1: Definitions of angle of attack, flight path angle.

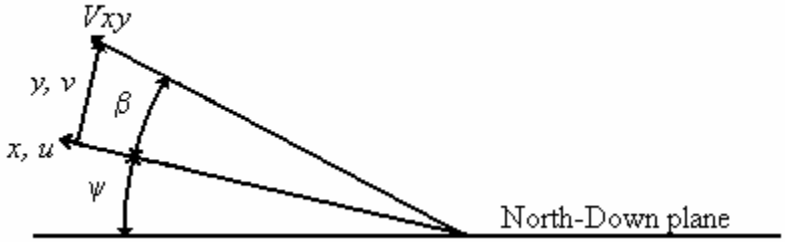

Figure 2.2: Definitions of sideslip angle and yaw angle.

Based on the body fixed velocities (u,v,w) the angle of attack (α) and the sideslip angle (β) are defined.

(2.1) $$\tan(\alpha) = \frac{w}{u}$$

(2.2) $$\sin(\beta) = \frac{v}{V}$$

2.2 Euler Angle Rates and Earth Fixed Velocities

In order to determine the velocity of the aircraft terms of an earth fixed frame (ECEF or geodetic) the orientation and position of the aircraft are written in terms of the *NED* frame. This necessitates a coordinate system rotation from the body fixed frame to the *NED* frame. The necessary transformation is taken as a series of rotations, commonly referred to as a 3-2-1 Euler angle sequence [2] and [3].

1. Rotate the body frame about the body down axis (z_b) by the heading angle (ψ), this results in the '1' frame ($x_1 y_1 z_1$). $[R_3]_\psi$
2. Rotate the 1 frame ($x_1 y_1 z_1$) about the '1' right axis (y_1) by the attitude angle (θ), this results in the '2' frame ($x_2 y_2 z_2$). $[R_2]_\theta$

3. Rotate the 2 frame ($x_2 y_2 z_2$) about the '2' forward axis (x_2) by the bank angle (ϕ), this results in the body fixed frame ($x_b y_b z_b$). $[R_1]_\phi$

By combining the coordinate rotations in the appropriate sequence the aircraft velocity in the body frame (u,v,w) is determined as a function of Euler angles (ψ,θ,ϕ) and *NED* frame velocity ($\dot{N},\dot{E},\dot{D}$).

$$\begin{bmatrix} u \\ v \\ w \end{bmatrix} = [R_1]_\phi [R_2]_\theta [R_3]_\psi \begin{bmatrix} \dot{N} \\ \dot{E} \\ \dot{D} \end{bmatrix}$$

$$\begin{bmatrix} u \\ v \\ w \end{bmatrix} = \begin{bmatrix} 1 & 0 & 0 \\ 0 & \cos(\phi) & \sin(\phi) \\ 0 & -\sin(\phi) & \cos(\phi) \end{bmatrix} \begin{bmatrix} \cos(\theta) & 0 & -\sin(\theta) \\ 0 & 1 & 0 \\ \sin(\theta) & 0 & \cos(\theta) \end{bmatrix} \begin{bmatrix} \cos(\psi) & \sin(\psi) & 0 \\ -\sin(\psi) & \cos(\psi) & 0 \\ 0 & 0 & 1 \end{bmatrix} \begin{bmatrix} \dot{N} \\ \dot{E} \\ \dot{D} \end{bmatrix}$$

(2.3)

$$\begin{bmatrix} u \\ v \\ w \end{bmatrix} = \begin{bmatrix} \cos(\psi)\cos(\theta) & \cos(\theta)\sin(\psi) & -\sin(\theta) \\ \cos(\psi)\sin(\theta)\sin(\phi) - \sin(\psi)\cos(\phi) & \sin(\psi)\sin(\theta)\sin(\phi) + \cos(\psi)\cos(\phi) & \cos(\theta)\sin(\phi) \\ \cos(\psi)\sin(\theta)\cos(\phi) + \sin(\psi)\sin(\phi) & \sin(\psi)\sin(\theta)\cos(\phi) - \cos(\psi)\sin(\phi) & \cos(\theta)\cos(\phi) \end{bmatrix} \begin{bmatrix} \dot{N} \\ \dot{E} \\ \dot{D} \end{bmatrix}$$

Inverting the rotation matrix yields the fixed frame velocities ($\dot{N},\dot{E},\dot{D}$) in terms of the Euler angles (ψ,θ,ϕ) and the body fixed velocities (u,v,w).

(2.4)

$$\begin{bmatrix} \dot{N} \\ \dot{E} \\ \dot{D} \end{bmatrix} = \begin{bmatrix} \cos(\theta)\cos(\psi) & \sin(\phi)\sin(\theta)\cos(\psi) - \cos(\phi)\sin(\psi) & \cos(\phi)\sin(\theta)\cos(\psi) + \sin(\phi)\sin(\psi) \\ \cos(\theta)\sin(\psi) & \sin(\phi)\sin(\theta)\sin(\psi) + \cos(\phi)\cos(\psi) & \cos(\phi)\sin(\theta)\sin(\psi) - \sin(\phi)\cos(\psi) \\ -\sin(\theta) & \sin(\phi)\cos(\theta) & \cos(\phi)\cos(\theta) \end{bmatrix} \begin{bmatrix} u \\ v \\ w \end{bmatrix}$$

In addition, the Euler angle rates ($\dot{\psi},\dot{\theta},\dot{\phi}$) are related to the body fixed angular velocities (p,q,r), [2] and [3].

(2.5)
$$\begin{bmatrix} \dot{\phi} \\ \dot{\theta} \\ \dot{\psi} \end{bmatrix} = \begin{bmatrix} 1 & \sin(\phi)\tan(\theta) & \cos(\phi)\tan(\theta) \\ 0 & \cos(\phi) & -\sin(\phi) \\ 0 & \sin(\phi)\sec(\theta) & \cos(\phi)\sec(\theta) \end{bmatrix} \begin{bmatrix} p \\ q \\ r \end{bmatrix}$$

The guidance control algorithms, Section 4, use (2.4) and (2.5) to track the orientation, velocity, and position of the aircraft.

2.3 Forces and Moments

Rigid body aircraft dynamics is analyzed separately in terms of the aircraft rotational and translational motion. Rotational motion is characterized by rotation of the aircraft about the body axis (x_b,y_b,z_b) expressed in terms of the angular rates (p,q,r) and moments (L,M,N). Translational motion is characterized by translation in the directions of the body axis (x_b,y_b,z_b) expressed in terms of velocities (u,v,w) and forces (X,Y,Z).

The rigid body equations of motion are derived from Newton's second law [3]. Assuming the aircraft is symmetric about the x_b,z_b plane, the body forces (X,Y,Z) and Moments (L,M,N) are derived, [2] and [3].

$$\begin{aligned} X &= m(\dot{u} + qw - rv) \\ Y &= m(\dot{v} + ru - pw) \\ Z &= m(\dot{w} + pv - qu) \end{aligned} \tag{2.6}$$

$$\begin{aligned} L &= I_{xx}\dot{p} - I_{xz}\dot{r} + qr(I_{zz} - I_{yy}) - I_{xz}pq \\ M &= I_{yy}\dot{q} + rp(I_{xx} - I_{zz}) + I_{xz}(p^2 - r^2) \\ N &= -I_{xz}\dot{p} + I_{zz}\dot{r} + pq(I_{yy} - I_{xx}) + I_{xz}qr \end{aligned} \tag{2.7}$$

2.4 Equations of Motion

Gravitational forces will have a net force effect acting at the center of mass of the aircraft. Gravitational attraction is assumed to be directed in the down direction (D). Applying the coordinate transformation described in Section 2.2 the forces due to gravity are written in the xyz frame.

$$\begin{aligned} X_{gravity} &= -mg\sin(\theta) \\ Y_{gravity} &= mg\cos(\theta)\sin(\phi) \\ Z_{gravity} &= mg\cos(\theta)\cos(\phi) \end{aligned} \tag{2.8}$$

To simplify the modeling and implementation of the general equations of motion the equations are linearized about a reference flight condition. Each variable in the equations of motion is written as a nominal value plus a perturbation. Equation 2.9 depicts an example of this for the forward body force (X). Generally, as will be assumed here, the reference flight conditions are taken to be steady-level flight.

(2.9) $X = X_o + \Delta X$

The linearized equations of motion are formulated from Equation 2.6 and Equation 2.7 by combining them with the gravitational forces, Equation 2.8, and ignoring products of perturbation variables, as shown in [1] and [2]. The body fixed force perturbations ($\Delta X, \Delta Y, \Delta Z$) and moments ($\Delta L, \Delta M, \Delta N$) are written by chain rule expansion relative to the perturbation variables. Negligible terms have been dropped in Equation 2.10 and Equation 2.11, [2].

$$\Delta X = \frac{\partial X}{\partial u}\Delta u + \frac{\partial X}{\partial w}\Delta w + \frac{\partial X}{\partial \delta_e}\Delta\delta_e$$

(2.10)
$$\Delta Y = \frac{\partial Y}{\partial v}\Delta v + \frac{\partial Y}{\partial p}\Delta p + \frac{\partial Y}{\partial r}\Delta r + \frac{\partial Y}{\partial \delta_r}\Delta\delta_r$$

$$\Delta Z = \frac{\partial Z}{\partial u}\Delta u + \frac{\partial Z}{\partial w}\Delta w + \frac{\partial Z}{\partial \dot{w}}\Delta\dot{w} + \frac{\partial Z}{\partial q}\Delta q + \frac{\partial Z}{\partial \delta_e}\Delta\delta_e$$

$$\Delta L = \frac{\partial L}{\partial v}\Delta v + \frac{\partial L}{\partial p}\Delta p + \frac{\partial L}{\partial r}\Delta r + \frac{\partial L}{\partial \delta_r}\Delta\delta_r + \frac{\partial L}{\partial \delta_a}\Delta\delta_a$$

(2.11)
$$\Delta M = \frac{\partial M}{\partial u}\Delta u + \frac{\partial M}{\partial w}\Delta w + \frac{\partial M}{\partial \dot{w}}\Delta\dot{w} + \frac{\partial M}{\partial q}\Delta q + \frac{\partial M}{\partial \delta_e}\Delta\delta_e$$

$$\Delta N = \frac{\partial N}{\partial v}\Delta v + \frac{\partial N}{\partial p}\Delta p + \frac{\partial N}{\partial r}\Delta r + \frac{\partial N}{\partial \delta_r}\Delta\delta_r + \frac{\partial N}{\partial \delta_a}\Delta\delta_a$$

The longitudinal and lateral equations of motion are grouped separately and formed as a set of first-order differential equations as shown in Equation 2.12 below. This is possible due to the weak interaction between longitudinal and lateral dynamics in conventional aircraft, see [2].

(2.12) $\Delta\dot{\vec{x}} = [A]\Delta\vec{x} + [B]\Delta\vec{u}$

The matrices [A] and [B] are composed of constant coefficients related to the mass properties and aerodynamic characteristics of the airplane. Development and a description of the relevant equations and constants are included in Appendix C and Appendix D. The resulting equations are included here for completeness.

(2.13)

$$\begin{bmatrix} \Delta\dot{u} \\ \Delta\dot{w} \\ \Delta\dot{q} \\ \Delta\dot{\theta} \end{bmatrix} = \begin{bmatrix} X_u & X_w & 0 & -g \\ Z_u & Z_w & u_o & 0 \\ M_u + M_{\dot{w}} Z_u & M_w + M_{\dot{w}} Z_w & M_q + M_{\dot{w}} u_o & 0 \\ 0 & 0 & 1 & 0 \end{bmatrix} \begin{bmatrix} \Delta u \\ \Delta w \\ \Delta q \\ \Delta\theta \end{bmatrix} + \begin{bmatrix} X_{\delta_e} \\ Z_{\delta_e} \\ M_{\delta_e} + M_{\dot{w}} Z_{\delta_e} \\ 0 \end{bmatrix} \begin{bmatrix} \Delta\delta_e \end{bmatrix}$$

(2.14)

$$\begin{bmatrix} \Delta\dot{\beta} \\ \Delta\dot{p} \\ \Delta\dot{r} \\ \Delta\dot{\phi} \end{bmatrix} = \begin{bmatrix} \frac{Y_\beta}{u_o} & \frac{Y_p}{u_o} & \frac{Y_r}{u_o} - 1 & \frac{g\cos(\theta_o)}{u_o} \\ L_\beta & L_p & L_r & 0 \\ N_\beta & N_p & N_r & 0 \\ 0 & 1 & 0 & 0 \end{bmatrix} \begin{bmatrix} \Delta\beta \\ \Delta p \\ \Delta r \\ \Delta\phi \end{bmatrix} + \begin{bmatrix} \frac{Y_{\delta_a}}{u_o} & \frac{Y_{\delta_r}}{u_o} \\ L_{\delta_a} & L_{\delta_r} \\ N_{\delta_a} & N_{\delta_r} \\ 0 & 0 \end{bmatrix} \begin{bmatrix} \Delta\delta_a \\ \Delta\delta_r \end{bmatrix}$$

3 Orientation Control

The inner control loops of the system are responsible for determining the control surface deflections necessary to achieve a desired orientation. Longitudinal orientation is controlled by specifying a desired attitude angle (θ_s), inverting the dynamics to approximate the required elevator deflection (δ_e), and applying the elevator deflection (δ_e) to the forward dynamics. Lateral orientation is controlled in much the same way although two control surface deflections, aileron and rudder (δ_a,δ_r), are controlled to achieve the desired bank angle (ϕ) and sideslip angle (β). Simple representations of the longitudinal and lateral orientation control are shown in Figure 3.1 and Figure 3.2.

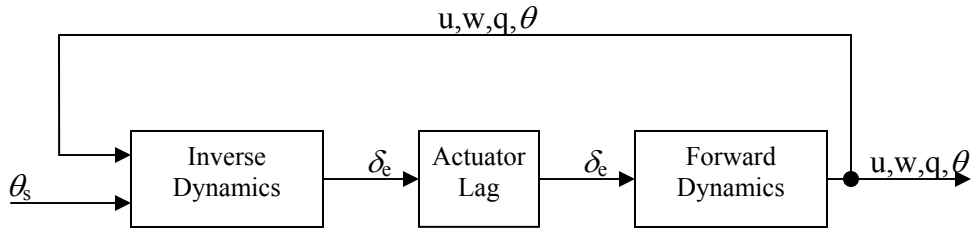

Figure 3.1: Longitudinal inner-loop orientation control loop.

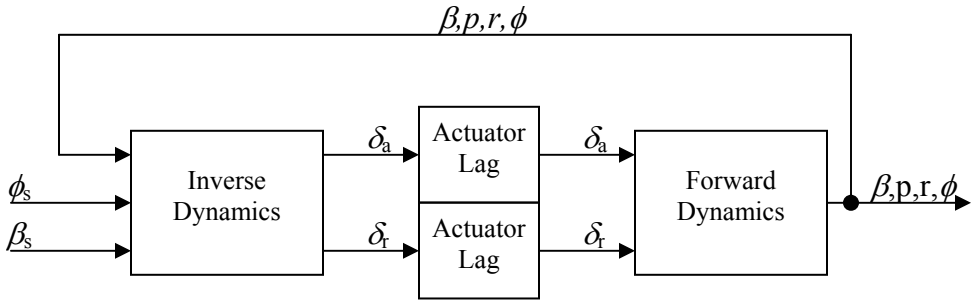

Figure 3.2: Lateral inner-loop orientation control loop.

3.1 Forward Dynamics

The forward dynamics of the inner-loop controls implement the equations of motion as derived in Section 2.4.

3.2 Inverse Dynamics

Dynamic inversion is a method of determining necessary control inputs by imposing a desired response characteristic to the system output. Recall the forward dynamics of the system are formed in a state-space representation.

(3.1) $\dot{\vec{x}} = [A]\vec{x} + [B]\vec{U}$ (Note the Δ symbol has been dropped)

If a control law of the form of Equation 3.2 is implemented the dynamics of the original system will be cancelled, assuming the control influence matrix (B) has an inverse. The result is a system response based on the imposed dynamics (A_d), [4] [5] [6].

(3.2) $\vec{U} = [B]^{-1}([A_d]\vec{x} - [A]\vec{x})$

$$\dot{\vec{x}} = [A]\vec{x} + [B][B]^{-1}([A_d]\vec{x} - [A]\vec{x})$$

$$\dot{\vec{x}} = [A_d]\vec{x}$$

3.2.1 Longitudinal Inversion

The response imposed upon the system is a second-order damped response.

$$\ddot{\theta} + 2\zeta\omega_n\dot{\theta} + \omega_n{}^2(\theta - \theta_s) = 0$$

For flight conditions near steady-level flight the attitude rate ($\dot{\theta}$) is nearly equal to the pitch rate (q).

(3.3) $\dot{q} + 2\zeta\omega_n q + \omega_n{}^2(\theta - \theta_s) = 0$

Based on the longitudinal state-space model, Equation 3.1, pitch acceleration ($\dot{q}$) is written in terms of the states (u,w,q,θ) and elevator defection (δ_e).

(3.4) $\dot{q} = A_{31}u + A_{32}w + A_{33}q + A_{34}\theta + B_{31}\delta_e$

The elevator deflection (δ_e) is determined by combining Equation 3.3 and Equation 3.4.

(3.5) $$\delta_e = -\frac{(A_{31}u + A_{32}w + A_{33}q + A_{34}\theta + 2\zeta\omega_n q + \omega_n{}^2(\theta - \theta_s))}{B_{31}}$$

Equation 3.5 provides a means of calculating the necessary control input (δ_e) to yield the desired response as specified by the natural frequency (ω_n), the damping ratio (ζ), and the desired attitude angle (θ_s).

3.2.2 Lateral Inversion

The derivation of the lateral dynamic inversion is similar in many respects to the longitudinal case. For the flight conditions of concern rudder deflection (δ_r) will be used to maintain zero sideslip (β), thus ensuring turn coordination. A first-order lag response is suitable for the control of sideslip (β). Bank angle (ϕ) is controlled by the influence of both the rudder deflection (δ_r) and the aileron defection (δ_a). A second-order damped response is imposed on the bank angle response.

A second-order damped response is imposed upon the bank angle (ϕ).

$$\ddot{\phi} + 2\zeta\omega_n\dot{\phi} + \omega_n{}^2(\phi - \phi_s) = 0$$

Near the nominal flight condition the bank rate ($\dot{\phi}$) is nearly equal to the roll rate (p).

$$\dot{p} + 2\zeta\omega_n p + \omega_n{}^2(\phi - \phi_s) = 0 \tag{3.6}$$

Based on the lateral state-space model the roll acceleration ($\dot{p}$) is written in terms of the states of the model (β,p,r,ϕ) and the control inputs (δ_r, δ_a).

$$\dot{p} = A_{21}\beta + A_{22}p + A_{23}r + A_{24}\phi + B_{21}\delta_a + B_{22}\delta_r \tag{3.7}$$

The aileron deflection (δ_a) is determined from Equation 3.6 and Equation 3.7.

$$\delta_a = -\frac{(A_{21}\beta + A_{22}p + A_{23}r + A_{24}\phi + B_{22}\delta_r + 2\zeta\omega_n p + \omega_n{}^2(\phi - \phi_s))}{B_{21}} \tag{3.8}$$

Thus the necessary control input (δ_a) is specified by the natural frequency (ω_n), the damping ratio (ζ), and the desired bank angle (ϕ_s).

A first-order lag is imposed to control the sideslip angle.

(3.9) $$\dot{\beta} = \frac{\beta_s - \beta}{\tau}$$

Based on the state-space model for the lateral system, sideslip angular rate ($\dot{\beta}$) is determined in terms of the states of the model and the control inputs (δ_r, δ_a):

(3.10) $$\dot{\beta} = A_{11}\beta + A_{12}p + A_{13}r + A_{14}\phi + B_{11}\delta_a + B_{12}\delta_r$$

Generally, aileron deflection (δ_a) has a negligible effect on sideslip rate ($\dot{\beta}$), thus the necessary rudder deflection (δ_r) is solved, [2].

(3.11) $$\delta_r = -\frac{(A_{11}\beta + A_{12}p + A_{13}r + A_{14}\phi - \frac{\beta_s - \beta}{\tau})}{B_{12}}$$

3.2.3 Actuator Lag

The response of each actuator to a commanded input is modeled as a simple first-order lag, Figure 3.3. For many purposes a first-order lag model would be an oversimplification, but for the purposes of this project it is considered adequate. Time constant values (τ) for each actuator and aircraft model are listed in Appendix C.

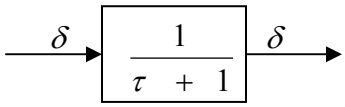

Figure 3.3: Actuator lag.

3.3 Flight Path Angle and Bank Angle

Two simple subsystems are employed to link the orientation control inputs (ψ_s, θ_s, ϕ_s) to the guidance control outputs ($\dot{h}_s, \dot{\psi}_s$). The guidance control system is decoupled into an altitude control loop and a heading control loop. Altitude control determines the desired altitude rate ($\dot{h}_s$). The heading control loop solves for the desired heading rate ($\dot{\psi}_s$). The transition between the inner-loop and outer-loop controls is depicted in Figure 3.4.

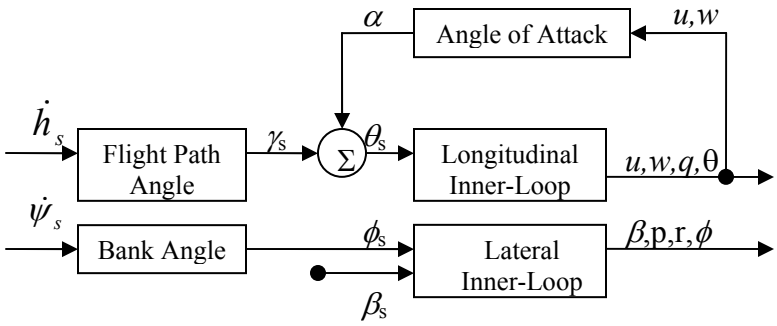

Figure 3.4: Conversion functions to link inner-loop control to outer-loop control.

3.3.1 Determining Desired Attitude Angle

Altitude is controlled by specifying a desired altitude rate ($\dot{h}_s$), calculating the desired flight path angle (γ_s), and the corresponding desired attitude angle (θ_s). The instantaneous angle of attack (α) is necessary to convert between the desired flight path angle (γ_s) and the desired attitude angle (θ_s).

$$\sin(\gamma_s) = \frac{\dot{h}_s}{u_0 + \Delta u}$$

$$\tan(\alpha) = \frac{w}{u_0 + \Delta u}$$

$$\theta_s = \gamma_s + \alpha = \sin^{-1}\left(\frac{\dot{h}_s}{u_0 + \Delta u}\right) + \tan^{-1}\left(\frac{w}{u_0 + \Delta u}\right)$$

3.3.2 Determining Desired Bank Angle

Heading is controlled by determining the desired heading rate ($\dot{\psi}_s$) and calculating the corresponding desired bank angle (ϕ_s). The general relation between desired bank angle (ϕ_s) and desired heading rate ($\dot{\psi}_s$) is determined by a simple force balance of a banked aircraft, Equation 3.12. Sideslip angle (β) has been neglected in Equation 3.12 by assuming its associated inner-loop controller is fast enough to maintaining it near zero.

(3.12) $$\phi_s = \tan^{-1}\left(\frac{(u_o + \Delta u)\dot{\psi}_s}{g}\right)$$

4 Guidance

Navigation and guidance of the aircraft is based on earth fixed reference frames. The Earth Fixed Earth Centered (ECEF) frame is a Cartesian system, centered on the earth, and rotates with the earth. The geodetic frame is a spherical coordinate frame which also rotates with earth and has its origin at earth's center. Position in the geodetic system is given in the familiar latitude (Λ), longitude (λ), and altitude (h) coordinates.

The guidance control represents the outer-loop control of the system, depicted as a block diagram in Figure 4.1. The earth normal and earth tangential kinematics of the system are decoupled into altitude and heading control loops, respectively. The desired trajectory is defined by great circle arcs between successive waypoints. The ability to guide the aircraft onto a desired trajectory is obviously dependent upon continuously tracking the position of the aircraft.

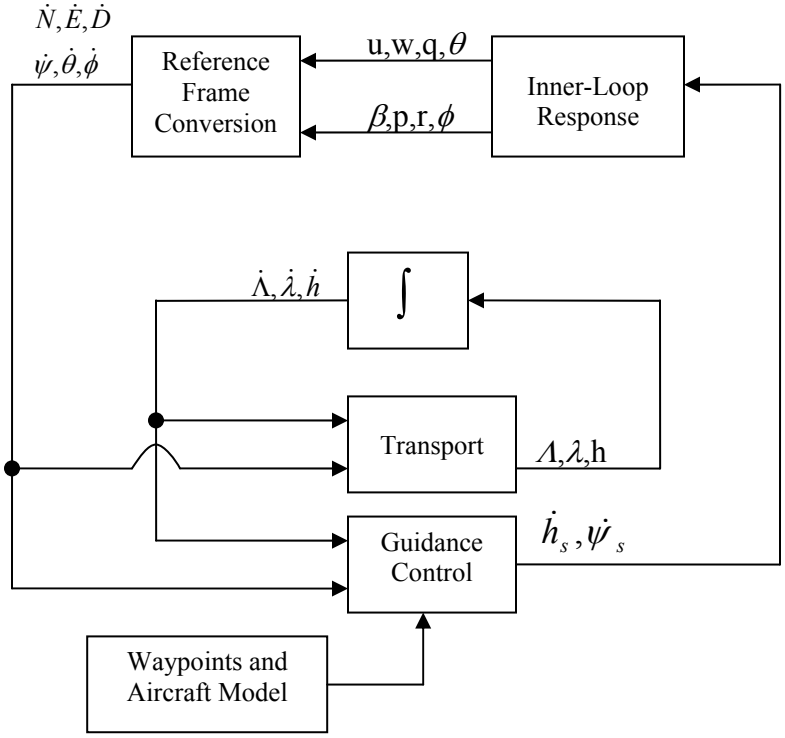

Figure 4.1: Guidance control loop.

4.1 Aircraft Transport

Aircraft position and orientation are imperative in order to control the aircraft onto a desired trajectory. The guidance system operates in terms of the earth fixed geodetic reference frame, requiring a reference frame transformation. The latitude and longitude rates ($\dot{\Lambda}, \dot{\lambda}$) are calculated from spherical geometry. Altitude rate ($\dot{h}$) is the same in magnitude and opposite in sign as the down rate ($\dot{D}$).

$$\dot{\Lambda} = \frac{\dot{N}}{R_e + h} \tag{4.1}$$

$$\dot{\lambda} = \frac{\dot{E}}{(R_e + h) * \cos(\Lambda)} \tag{4.2}$$

$$\dot{h} = -\dot{D} \tag{4.3}$$

The geodetic rates ($\dot{\Lambda}, \dot{\lambda}, \dot{h}$) are continuously integrated to yield the aircraft position. Orientation is similarly determined. Heading angle rate ($\dot{\psi}$) is integrated for heading angle (ψ). Attitude angle (θ) and bank angle (ϕ) are known states of the system.

4.2 Trajectory

Each leg of the desired path is defined by a great circle arc between two successive waypoints. By definition, if the earth is assumed spherical, the great circle arc is defined as the intersection of a plane defined by the waypoints and the center of the earth and a sphere whose radius is the radius of the earth plus the altitude of the aircraft.

For this project the earth has been assumed to be spherical. Many more accurate models of the earth's shape exist. For the purposes of developing an INS system it may be essential to use a more accurate earth model.

4.2.1 Cross-track Error

The cross-track error (e) is defined as the projected distance from the aircraft position to the great circle plane, Figure 4.2. Cross-track error (e) is most naturally derived in the

ECEF frame. Vectors originating from the center of the earth and terminating at the previous and next waypoints (V_p,V_n) define the great circle plane, written as a normal vector in Equation 4.4. Similarly a vector from the center of the earth to the aircraft position (V_c) is used to define the cross-track error (e), Equation 4.5.

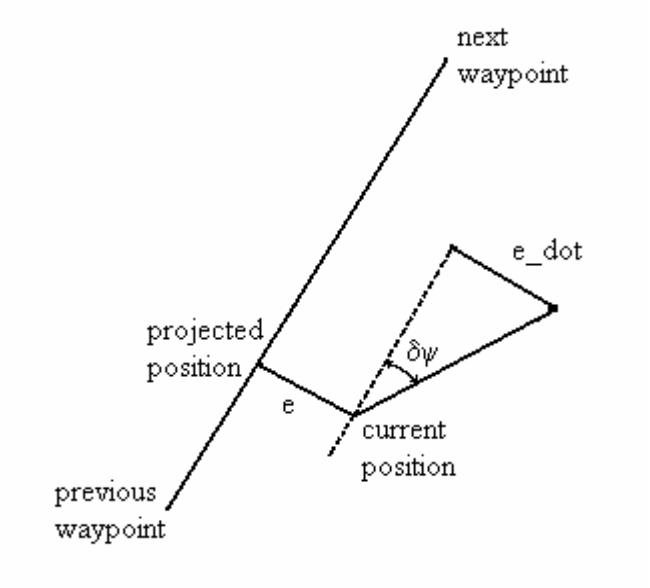

Figure 4.2: Graphical depiction of cross-track error and cross-track error rate.

(4.4) $$\hat{n} = \frac{\vec{V}_p}{|V_p|} \times \frac{\vec{V}_n}{|V_n|}$$

(4.5) $$e = \vec{V}_c \bullet \hat{n}$$

4.2.2 Cross-track Error Rate

There are several methods to calculate the cross-track error rate ($\dot{e}$). The method employed involves determination of the heading error (δ_ψ) from a nominal heading, referred to as the projected heading (ψ_{proj}). In this case the projected heading (ψ_{proj}) is defined as the heading of the aircraft position projected onto the great circle plane to the desired waypoint. Cross-track error rate ($\dot{e}$) is determined based on the geometry of Figure 4.2.

(4.6) $$\delta\psi = \psi_{proj} - \psi$$

(4.7) $$\dot{e} = \sqrt{\dot{N}^2 + \dot{E}^2} * \sin(\delta\psi)$$

4.2.3 Transition

Transition between successive legs of a desired trajectory is triggered by a minimum range to the next waypoint. The range limit (rng_{limit}) is determined as shown in Figure 4.3 by rearranging Equation 3.12 to form Equation 4.8. The turning radius of the aircraft (R) can be approximated by a heading rate ($\dot{\psi}_{\lim it}$) and the nominal velocity (u_0) of the aircraft. From the geometry of Figure 4.3 the range limit (rng_{limit}) is determined from the heading change between the two adjacent legs ($\Delta\psi$). Because a desired bank angle (ϕ_s) is not achieved instantaneously a constant is introduced in Equation 4.9 to account for the inherent delay.

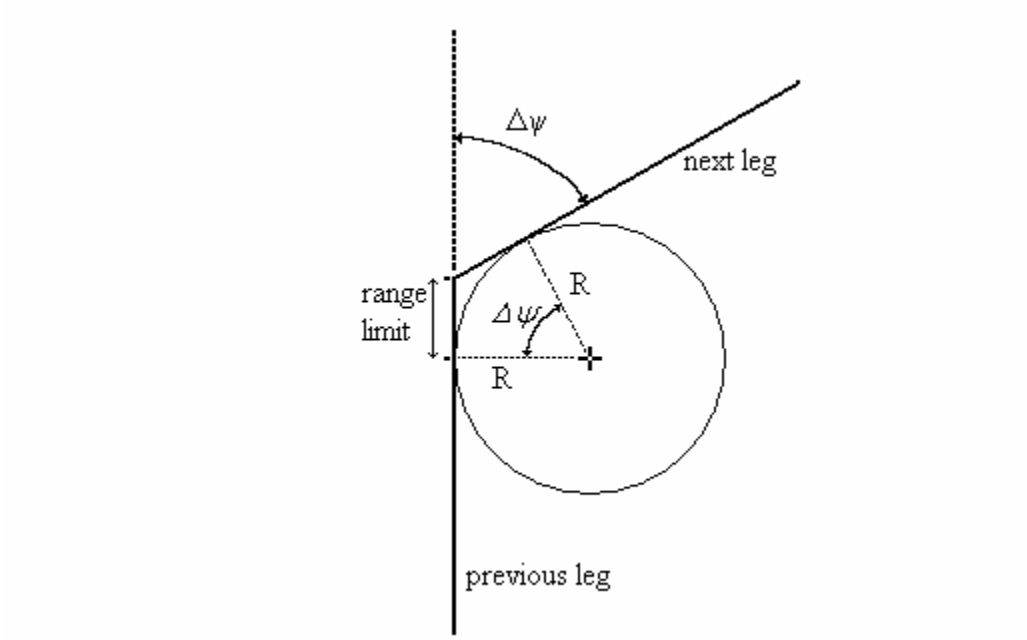

Figure 4.3: Graphical depiction of the range limit.

(4.8) $$\dot{\psi}_{\lim it} = \frac{g * \tan(\phi_{\lim it})}{u_0}$$

$$R = \frac{u_0}{\dot{\psi}_{\lim it}} = \frac{{u_0}^2}{g * \tan(\phi_{\lim it})}$$

$$rng_{\lim it} = R * \tan(\frac{\Delta\psi}{2})$$

(4.9) $$rng_{\lim it} = 1.7 * \frac{{u_0}^2}{g * \tan(\phi_{\lim it})} * \tan(\frac{\Delta\psi}{2})$$

4.3 Heading Control

The heading control laws are formulated based on a second-order system. The cross-track error acceleration ($\ddot{e}$) is determined by differentiating Equation 4.7. It is worth noting that although the true heading of the great circle arc is not constant along its path, the rate at which it changes is relatively small for the aircraft considered. Therefore, the heading error rate ($\dot{\delta}_{\psi}$) is approximately equal to the heading rate ($\dot{\psi}$). The second term of Equation 4.10 has been dropped for simplicity. Even though during transitions between path legs this quantity may become dominant, as will be shown later, neglecting this term still results in a controller with adequate performance.

$$\ddot{e} + 2\zeta\omega_n\dot{e} + \omega_n{}^2 e = 0$$

$$\ddot{e} = \sqrt{\dot{N}^2 + \dot{E}^2} * \cos(\delta_{\psi}) * \dot{\delta}_{\psi} + \frac{\partial\left(\sqrt{\dot{N}^2 + \dot{E}^2}\right)}{\partial t} * \sin(\delta_{\psi}) \tag{4.10}$$

$$\dot{\delta}_{\psi} = \dot{\psi}$$

$$\dot{\psi}_s = \frac{-2\zeta\omega_n\dot{e} + \omega_n{}^2 e}{\sqrt{\dot{N}^2 + \dot{E}^2} * \cos(\delta_{\psi})} \tag{4.11}$$

4.4 Altitude Control

For simplicity the desired altitude rate ($\dot{h}$) is determined by applying a time constant (τ) to the altitude error. In order for a diverse set of aircraft to yield similar altitude response characteristics the time constant (τ) is calculated based on a specified range constant (rng_{alt}).

$$\dot{h}_s = \frac{h_s - h}{\tau_{alt}} = \frac{h_s - h}{rng_{alt} * u_0} \tag{4.12}$$

5 Simulation

The Navion general aviation aircraft model as specified in [2] will be used to test the control systems. This model represents a moderately sized general aviation aircraft with a gross weight (W) of 2750 pounds and a nominal velocity (u_0) of 163 knots. The stability and control coefficients for the Navion, as well as several other aircraft, are provided in Appendix C.

Both longitudinal and lateral control will be analyzed by first simulating the orientation (inner-loop) control followed by simulation of the guidance (outer-loop) control system. Simulations were conducted using a Matlab/Simulink environment. Reasonable effort has been made to tune the control parameters to achieve fast rise times and little or no overshoot. Table B.1 contains parameter values for several aircraft including the values employed in the following examples.

5.1 Longitudinal Orientation Control

As stated in Section 3 the longitudinal orientation control loop utilizes the desired attitude angle (θ_s) as an input and outputs the longitudinal states (u,w,p,θ). Two parameters are used to tune the longitudinal orientation response, the natural frequency (ω_n) and damping ratio (ζ). For this analysis, the details of Section 3.3.1 and Section 4.4 will also be incorporated, this allows the desired altitude rate ($\dot{h}_s$) be used as the system input. By converting the results to the *NED* frame it is possible to directly compare the response down rate ($\dot{D}$) to the commanded altitude rate ($\dot{h}_s$).

A moderate decent rate of 600 ft per minute is commanded after 10 seconds of initially level flight. The response of the simulation is depicted in Figure A.1 and Figure A.2. Figure A.1 shows a down rate ($\dot{D}$) response characteristic of a second-order damped oscillator, similar to the imposed response. The down rate ($\dot{D}$) response quickly reaches a steady-state near 9 ft/s. This droop in response is attributed to lack of integral control

feedback. The altitude history of the simulation is also depicted in Figure A.1. In addition, the nonlinear response of the elevator deflection to the dynamic inversion is show in Figure A.1. Longitudinal sates (u,w,p,θ) are plotted in Figure A.2.

5.2 Altitude Control

Two waypoints (Λ,λ,h) are specified to analyze the longitudinal control. The first waypoint (0,0,0) specifies the initial condition of the aircraft. The second waypoint (0,0.25,-1000) sets the desired final position of the aircraft. For this simulation the critical component of the waypoints is the resulting commanded altitude change of 1000 feet. The only specified parameter, in addition to those required for the longitudinal orientation controller, is the range constant (rng_{alt}) as described in Section 4.4.

$$\text{waypoints: } \begin{bmatrix} 0 & 0 & 0 \\ 0 & 0.25 & -1000 \end{bmatrix}$$

Figure A.3 and Figure A.4 depict the same outputs as Figure A.1 and Figure A.2, respectively. The altitude history shows that the aircraft altitude converges as an exponential decay to the commanded altitude.

5.3 Lateral Orientation Control

The lateral orientation control loop outputs the lateral states (β,q,r,ϕ) provided a desired bank angle (ϕ_s) and a desired sideslip angle (β_s). Similar to the longitudinal case, it is preferred to compute the desire bank angle (ϕ_s) based on a desired heading rate ($\dot{\psi}_s$). Several parameters are tuned to specify the imposed dynamics for both the rudder and aileron. The desired sideslip angle (β_s) is set to zero for all cases studied for this project. The rudder time constant (τ), the aileron natural frequency (ω_n), and the aileron damping ratio (ζ) are tunable parameters.

After 10 seconds of level flight a 5 degrees per second heading rate ($\dot{\psi}_s$) is commanded. This translates to about a 25 degree desired bank angle (ϕ_s) by Equation 3.12. The simulated heading rate response is plotted in Figure A.5. The lack of integral action

control shows a droop in response to the commanded heading rate ($\dot{\psi}_s$) similar to the longitudinal orientation control. Also similar to the longitudinal case the control inputs, aileron deflection (δ_a) and rudder deflection (δ_r), show nonlinear characteristic.

Figure A.6 shows the response of the lateral state (β,q,r,ϕ). The sideslip angle (β) develops a maximum of only 0.015 degrees, affirming the assumption that the sideslip angle (β) is negligible.

5.4 Heading Control

Analysis of the heading control system requires specifying at least three waypoints. The first waypoint specifies the initial condition of the aircraft. The second waypoint defines an intermediate position and the third waypoint defines the desired final position of the aircraft. The selected waypoints represent a 90 degree heading change. Two parameters are required to tune the heading control response, natural frequency (ω_n) and damping ratio (ζ).

$$\text{waypoints: } \begin{bmatrix} 0 & 0 & 0 \\ 0 & 0.05 & 0 \\ -0.05 & 0.05 & 0 \end{bmatrix}$$

The response of the system is shown in Figure A.7 and Figure A.8. The heading response shows a damped second-order response as imposed on the system. Figure A.8 again reaffirms the small sideslip angle (β) assumption. Figure A.9 shows the aircraft track plotted along with the desired path.

5.5 Long-Period Simulation

The entire guidance system is also simulated in a full navigation and guidance simulation. For this simulation a series of seven waypoints are specified in the Mediterranean Sea. The waypoints represent a path from the Straits of Gibraltar to the Suez Canal [7].

$$\text{waypoints:} \begin{bmatrix} 36.00 & -5.00 & 0 \\ 36.00 & -2.00 & 1000 \\ 38.00 & 5.00 & 2500 \\ 38.00 & 11.00 & 1500 \\ 35.00 & 13.00 & 0 \\ 33.00 & 30.00 & 1000 \\ 31.50 & 32.00 & 0 \end{bmatrix}$$

The response path of the simulation is plotted with the local coast in Figure A.10. Figure A.11 shows a section of the flight path focused on waypoints 4, 5, and 6. The focused view of Figure A.11 and the heading history of Figure A.12 indicate that the aircraft is following a great circle route; this is particularly noticeable between waypoints 5 and 6.

5.6 Diverse Aircraft

For comparison the response of a Convair 880 passenger jet has also been simulated. Though still conventional, the Convair presents a very different aircraft than the Navion. The Convair 880 was developed as a competitor to the venerable Boeing 707. It has a gross weight (W) of 126,000 pounds and a cruise speed (u_0) of 396.5 knots (Mach .80). Both the orientation and guidance control gains for the Convair are the same as those used to control the Navion. The Convair's altitude guidance control response is plotted in Figure A.13 and Figure A.14. The heading control response is plotted in Figure A.15 and Figure A.16. The waypoints used for the heading simulation were modified such that the time required to fly along each leg was been held constant.

$$\text{Altitude simulation waypoints:} \begin{bmatrix} 0 & 0 & 0 \\ 0 & 0.25 & -1000 \end{bmatrix}$$

$$\text{Heading simulation waypoints:} \begin{bmatrix} 0 & 0 & 0 \\ 0 & 0.19 & 0 \\ -0.19 & 0.19 & 0 \end{bmatrix}$$

The altitude history and down rate response of the Convair closely matches the response of the Navion despite the fact that the characteristics of the states response differ greatly. The heading simulation has a similar response characteristic although the Convair quickly achieved the limited bank angle of 30 degrees.

6 Conclusion

The goal of this project was to develop a method of generating realistic aircraft velocities and rotation rates based on specification of a desired path in an spherical earth based coordinate system. Section 5 showed that the control systems developed are successful in generating aircraft trajectories given a series of waypoints. The control scheme has also been developed to control a diverse set of aircraft; this ability has been partially shown in Section 5.6.

The control scheme used in this project has several advantages over traditional control schemes such as a proportional-derivative (P-D) control scheme. The tunable parameters, such as natural frequencies and damping ratios, of these control systems generally have a more intuitive physical meaning than the gains of a P-D controller. The relation between the control parameters and the output of the controller also makes selecting and tuning the parameters quite simple.

6.1 Future Direction

The Matlab/Simulink model has been developed to be flexible, making modification very easy. Several simple and useful modifications can be implemented into the model to enhance performance. Integral action could be beneficial to aid the convergence of both the heading and altitude control. To make the simulation more realistic, rate and deflection limits could easily be placed on the commanded control deflections.

Several limitations have also been imposed by the models available in [2]. The lack of thrust control coefficients results in a velocity of the aircraft that is more passive than a realistic aircraft.

Linearization limits the range that the equations of motion are valid. The model's range of validity could be greatly expanded by not linearizing the equations of motion. This would also require re-formulation of the dynamic inversion controllers.

Appendix A Simulation Results

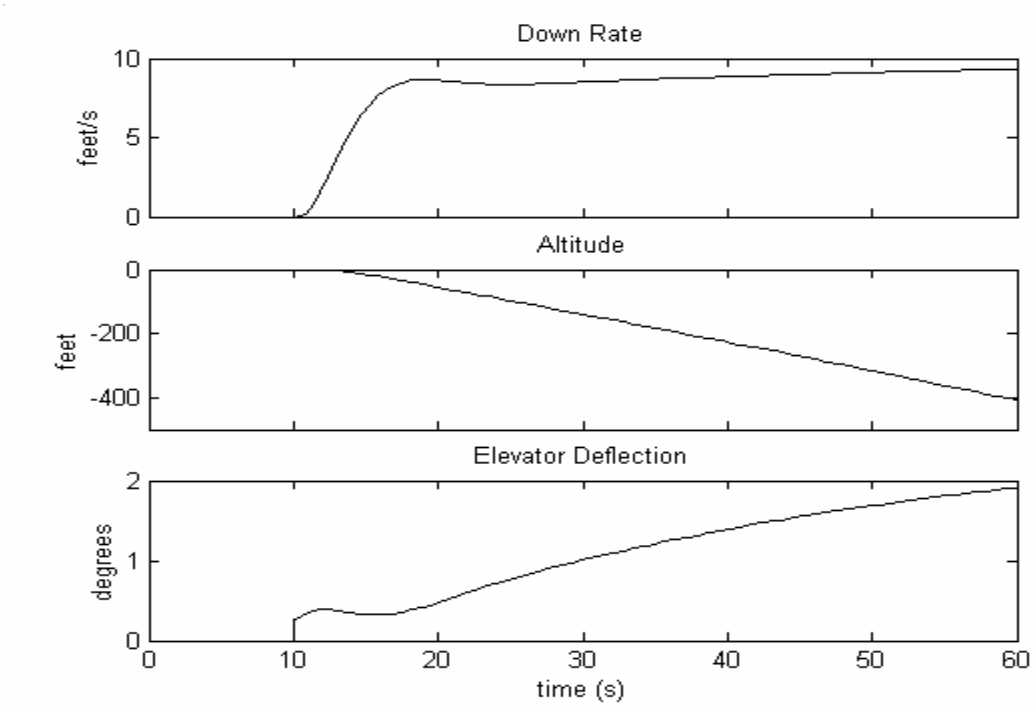

Figure A.1: Navion longitude orientation control response

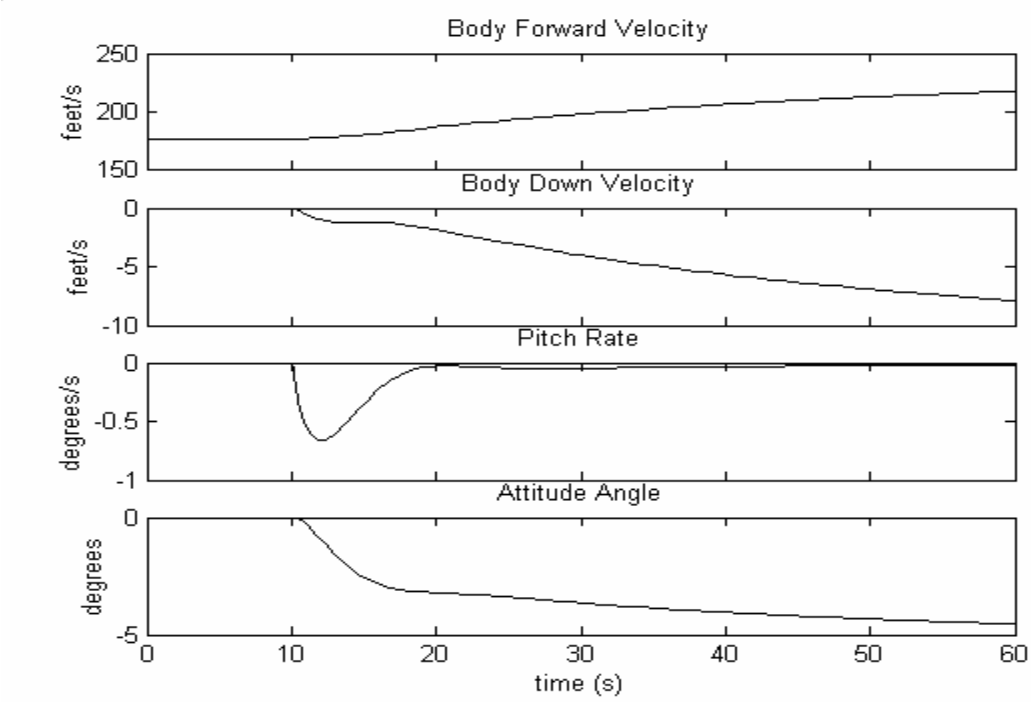

Figure A.2: Navion longitude orientation control response, states

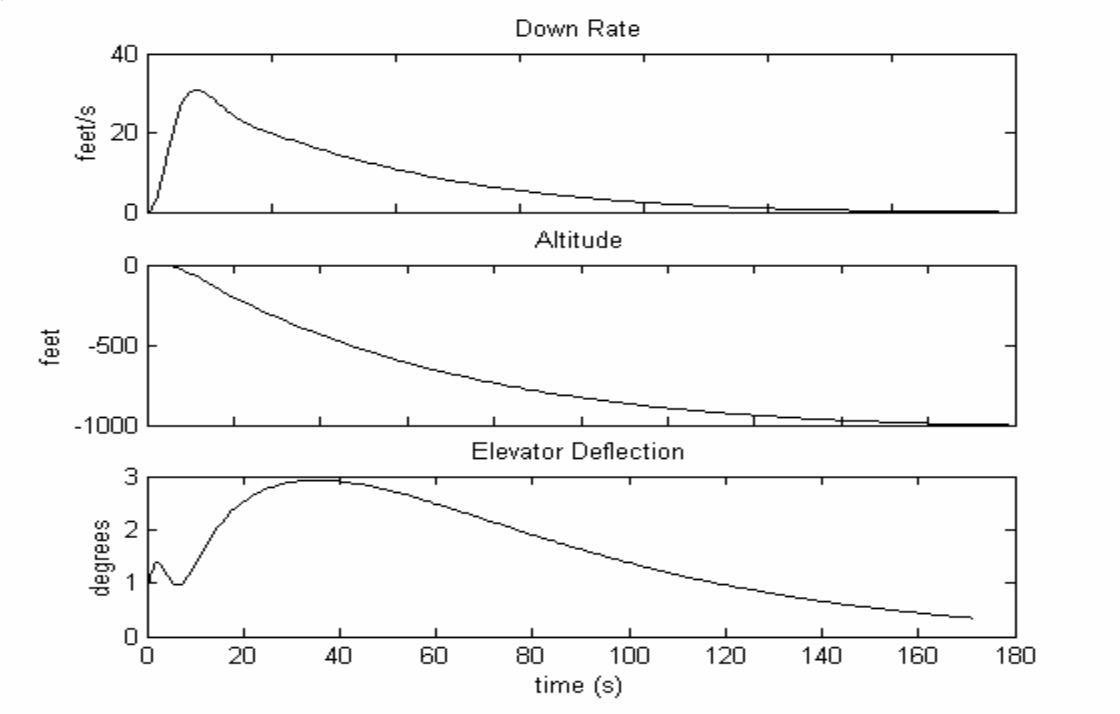

Figure A.3: Navion altitude guidance control response

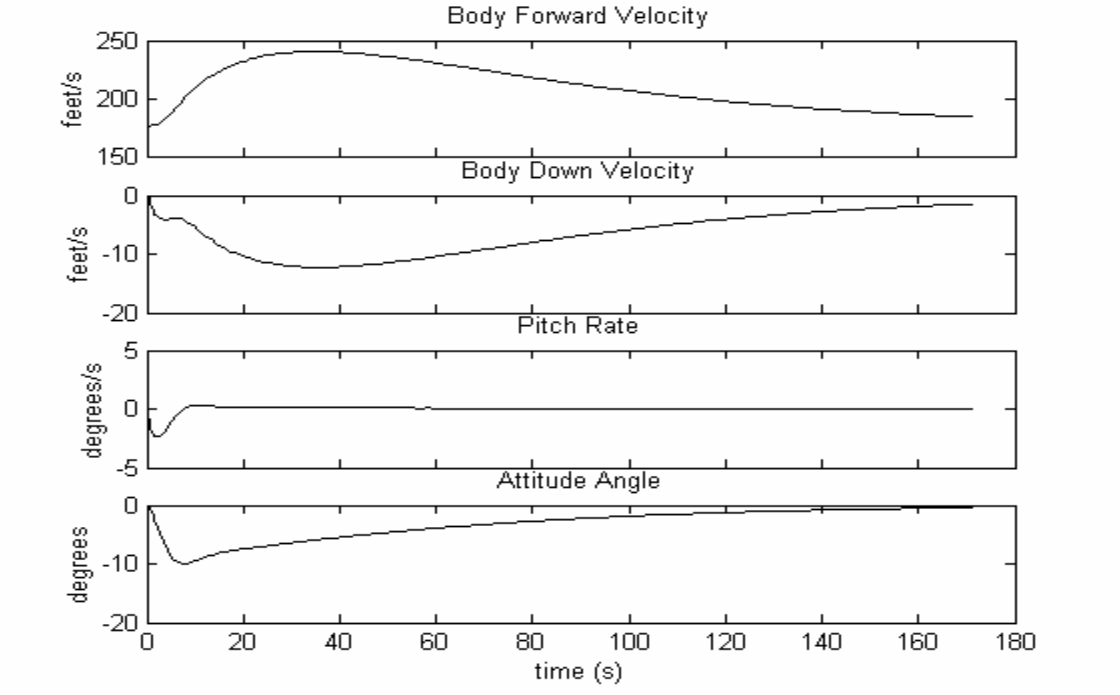

Figure A.4: Navion altitude guidance control response, states

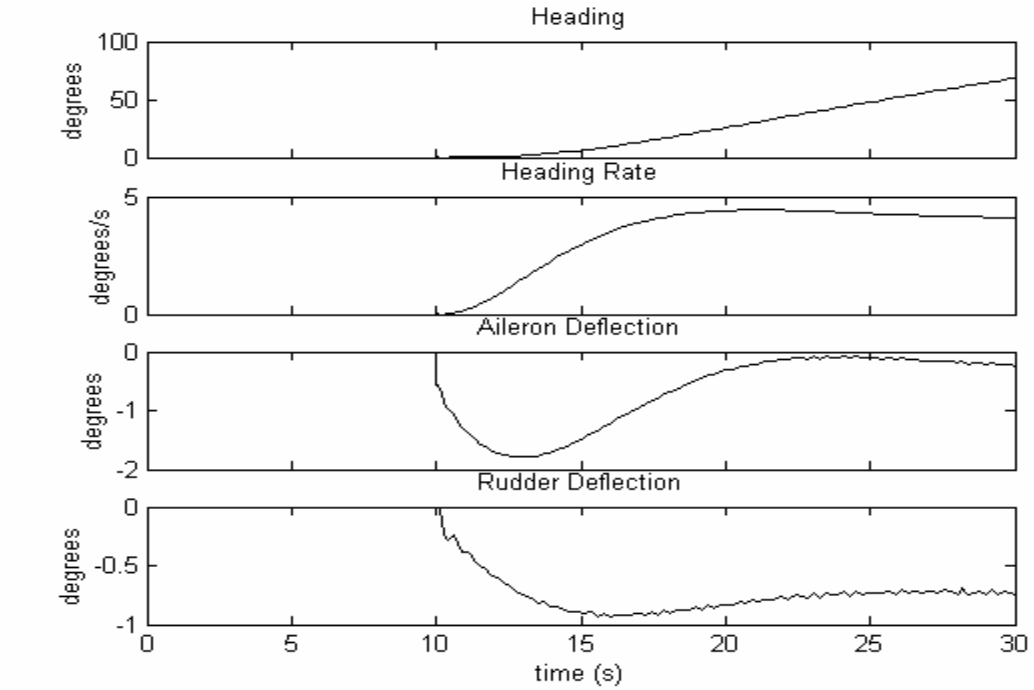

Figure A.5: Navion latitude orientation control response

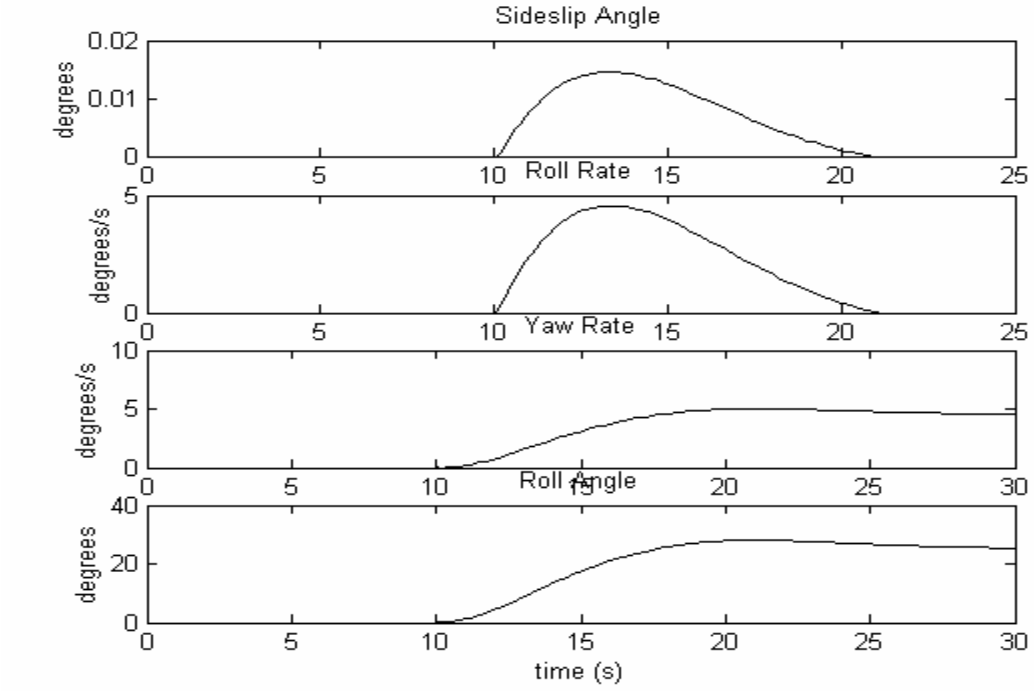

Figure A.6: Navion latitude orientation control response, states

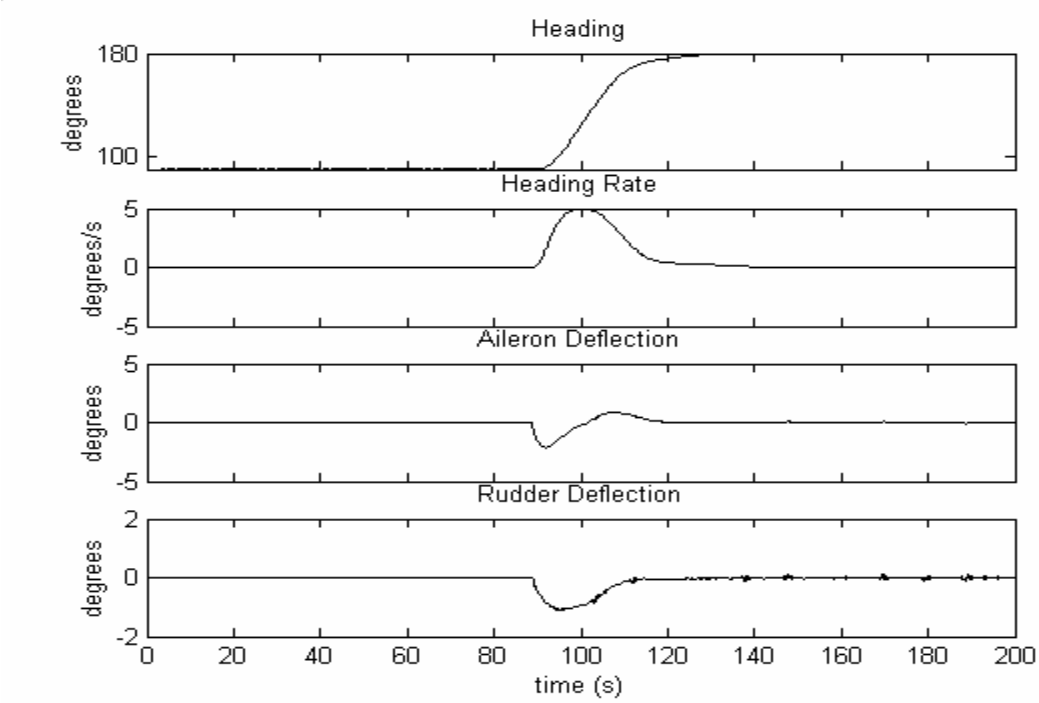

Figure A.7: Navion heading guidance control response

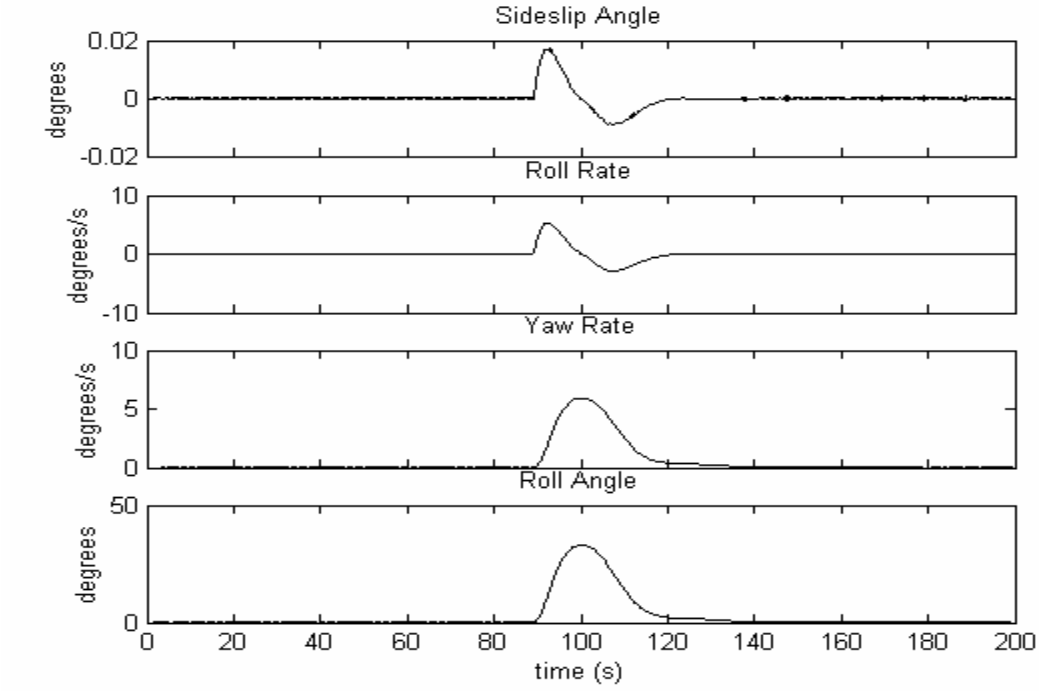

Figure A.8: Navion heading guidance control response, states

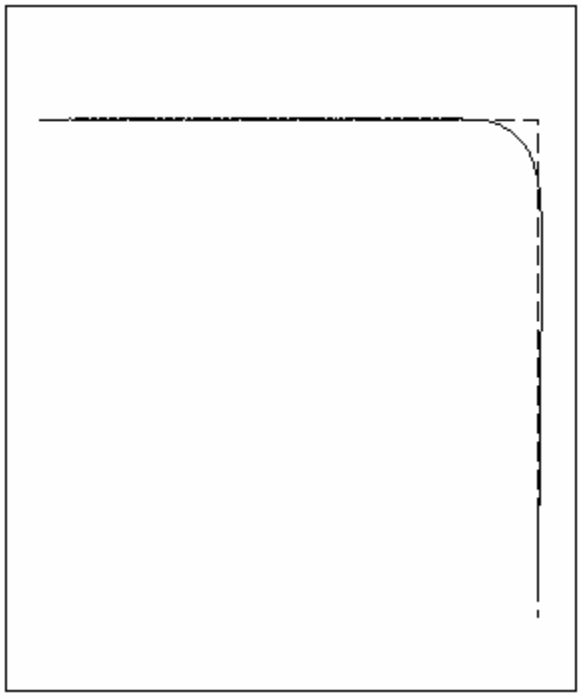

Figure A.9: Navion heading guidance control response, track

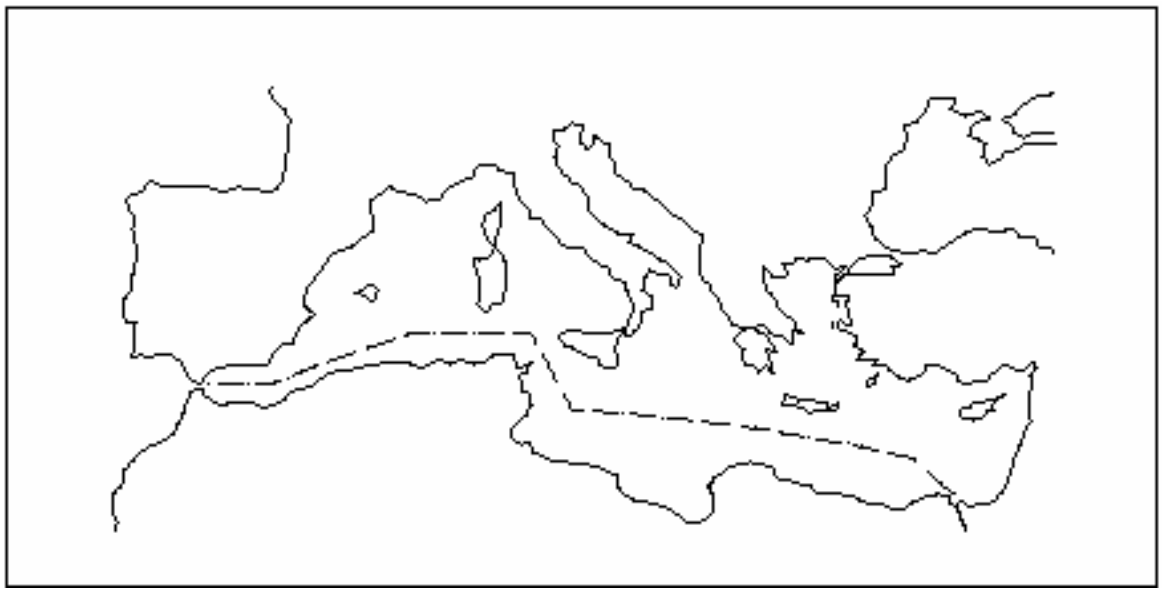

Figure A.10: Navion long-period simulation, response path

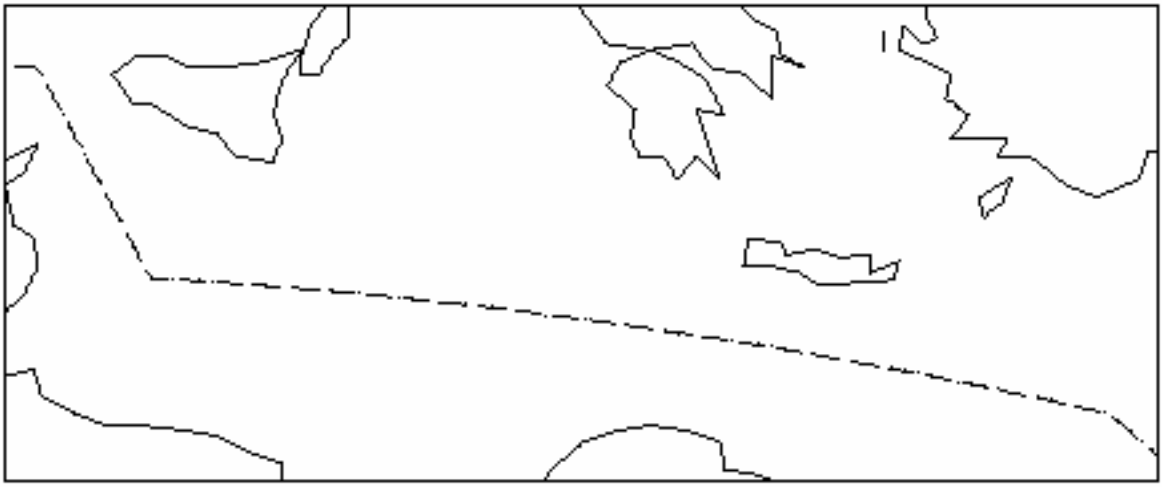

Figure A.11: Navion long-period simulation, response path focused on waypoints 4, 5, and 6

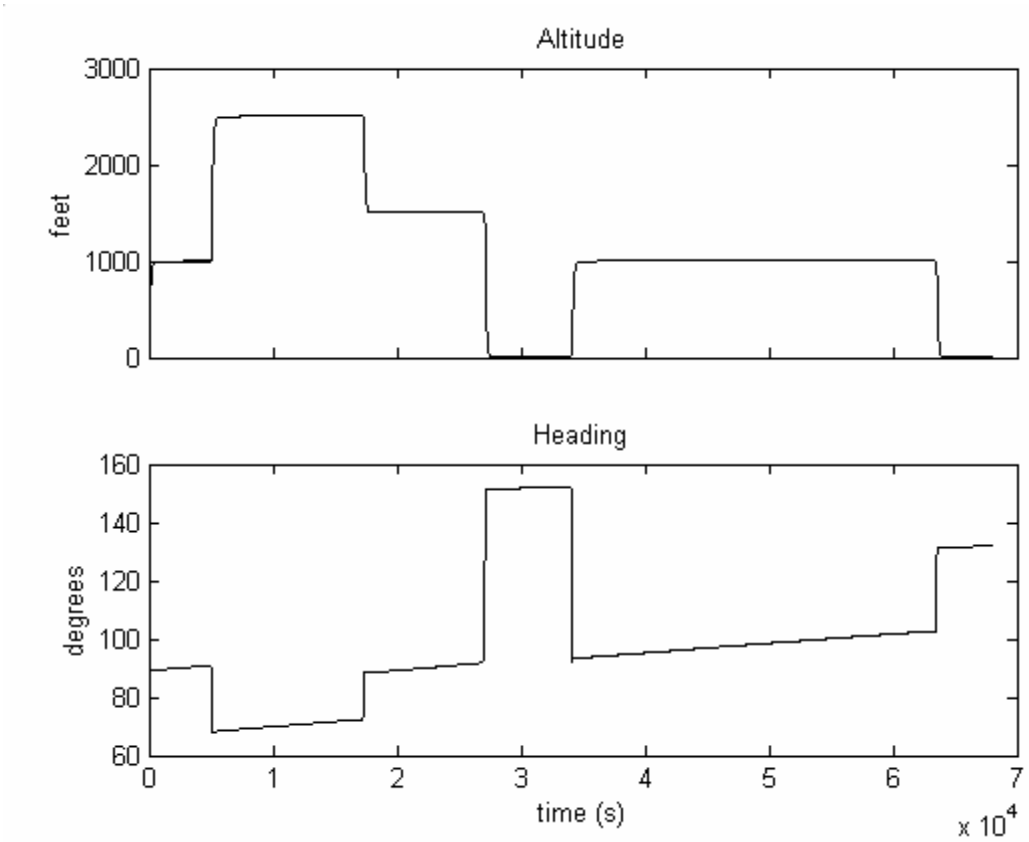

Figure A.12: Navion long-period simulation, altitude and heading response

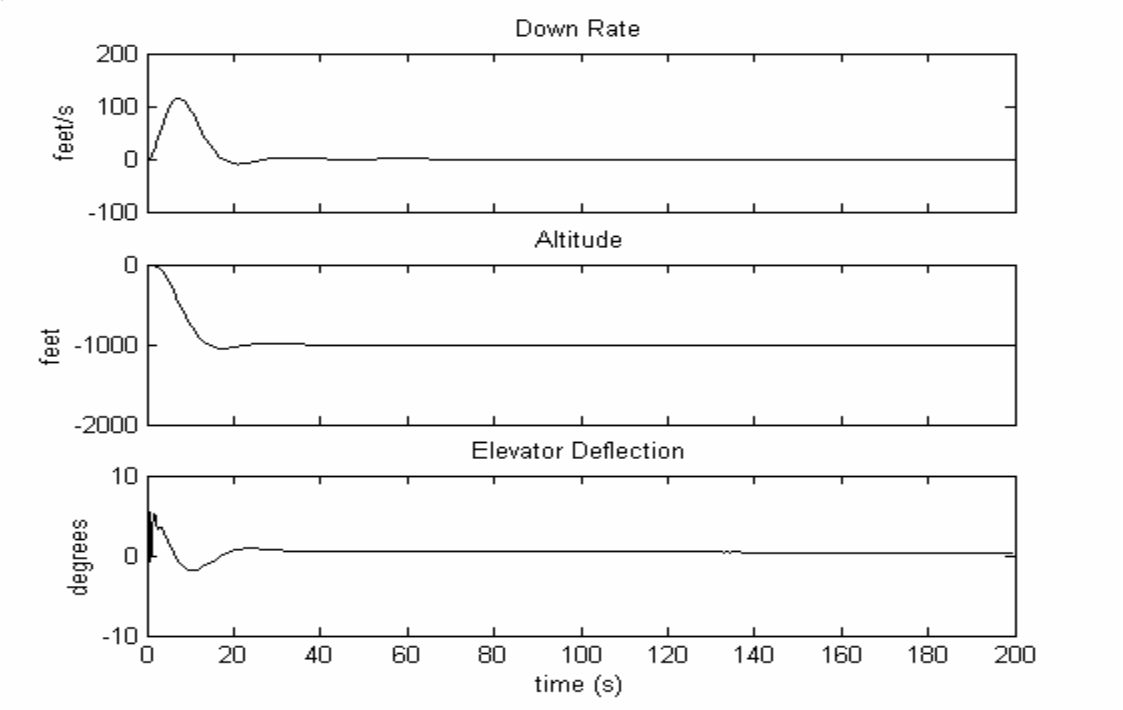

Figure A.13: Convair altitude guidance control response

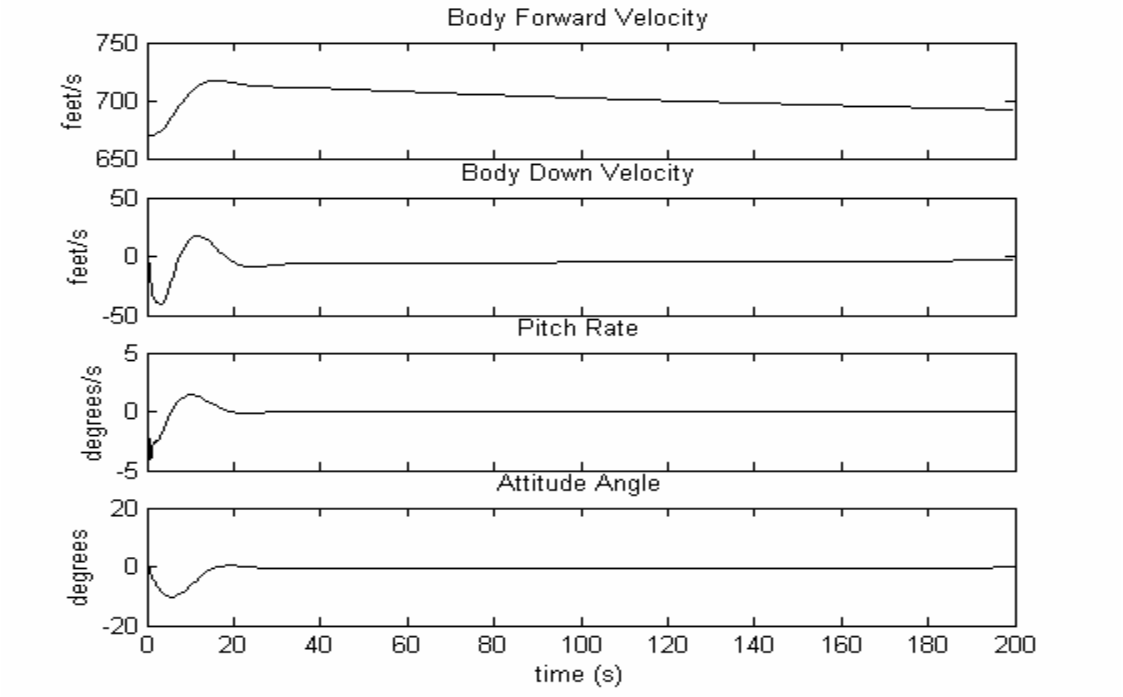

Figure A.14: Convair altitude guidance control response, states

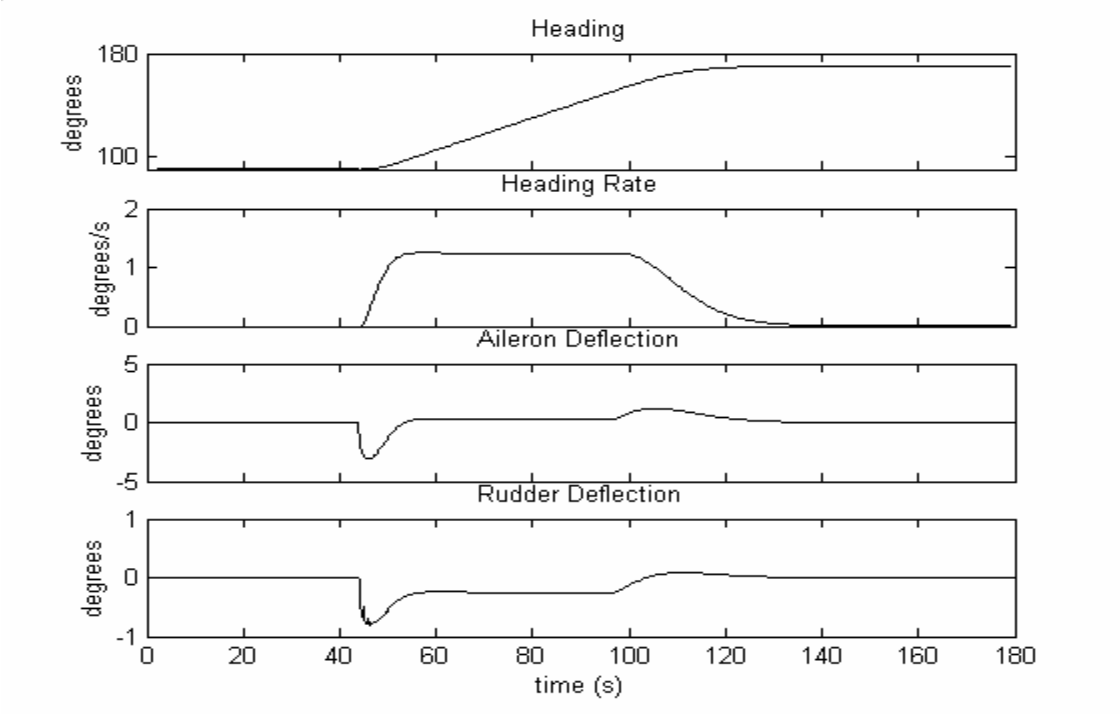

Figure A.15: Convair heading guidance control response

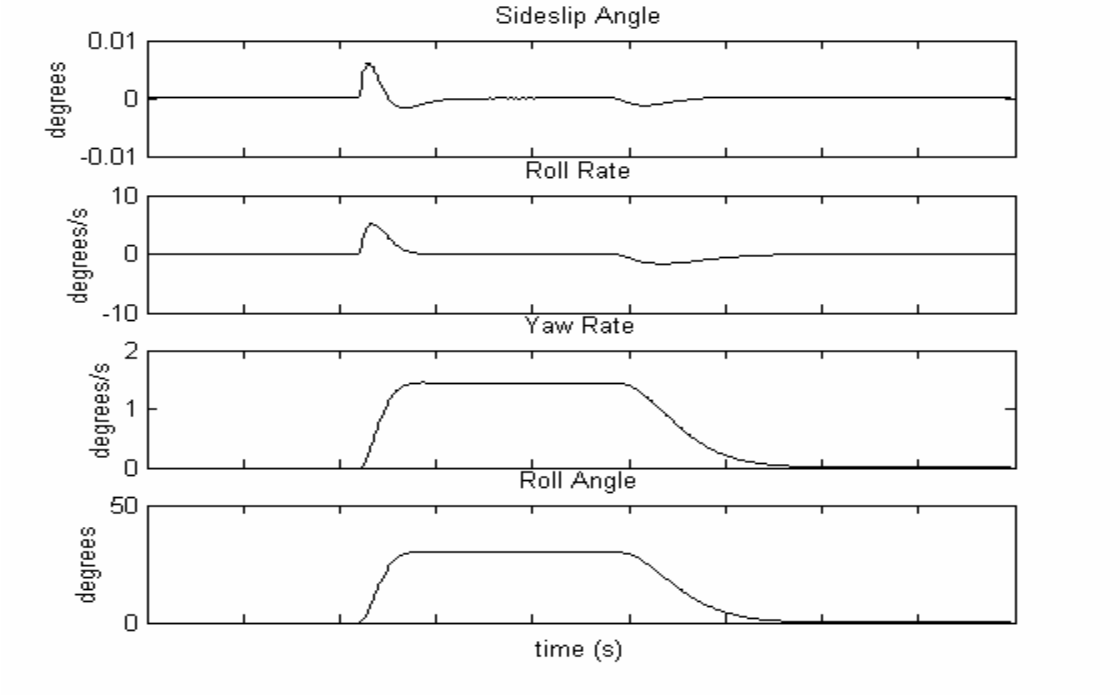

Figure A.16: Convair heading guidance control response, states

Appendix B Control Gains

The control gains of Table B.1 have been selected to yield quick responses and little or no overshoot of the desired parameter. Parameters were selected on a trial and error basis using the simulations described in Section 5. The similarity of the aircraft control parameters across all the aircraft models made the selection of parameters much easier.

	Boeing 747 M=.25	Boeing 747 M=.90	Convair M=.20	Convair M=.80	F104a M=.257	Jetstar M=.20	Navion
Altitude:							
rng_{alt}	5000	5000	5000	5000	5000	5000	5000
Heading:							
ω_n	0.05	0.05	0.05	0.05	0.05	0.05	0.05
ζ	0.9	0.9	0.9	0.9	0.9	0.9	0.9
Longitude:							
ω_n	1.4	1.4	1.4	1.4	1.0	0.6	1.0
ζ	3.0	2.4	3.0	2.4	2.0	2.0	1.8
Latitude:							
ω_n	1	1	1	1	1	1	0.8
ζ	2.1	2.1	2.1	2.1	2.1	2.1	1.5
τ	3	3	3	3	3	3	3
Actuator Time Constants:							
rudder:	0.5	0.5	0.5	0.5	0.5	0.5	0.5
elevator:	0.5	0.5	0.5	0.5	0.5	0.5	0.5
aileron:	0.5	0.5	0.5	0.5	0.5	0.5	0.5

Table B.1: Aircraft Control Gains

Appendix C Stability Coefficients

Stability coefficients for several aircraft are included in [2]; several of these models are included here for reference. Table C.1 lists some basic physical parameters for each aircraft. Table C.2 includes the stability and control coefficients that define the basis for the development of the state-space equations of motion, Appendix D.

	Boeing 747	Boeing 747	Convair	Convair	F104a	F104a	Navion
Mach Nominal altitude (ft)	0.25 0	0.9 40000	0.25 0	0.8 35000	0.257 0	1.8 55000	0.158 0
W (lbs)	636600	636600	126000	126000	16300	16300	2750
Ix (slug ft^2)	18200000	18200000	115000	115000	3549	3549	1048
Iy (slug ft^2)	33100000	33100000	2450000	2450000	58611	58611	3000
Iz (slug ft^2)	49700000	49700000	4070000	4070000	59669	59669	3530
Ixz (slug ft^2)	970000	970000	0	0	0	0	0
S (ft^2)	5500	5500	2000	2000	196.1	196.1	184
b (ft)	195.68	195.68	120	120	21.94	21.94	33.4
c (ft)	27.31	27.31	18.94	18.94	9.55	9.55	5.7

Table C.1: Aircraft Physical Parameters

	Boeing 747	Boeing 747	Convair	Convair	F104a	F104a	Navion
Longitudinal:							
CL_0	1.11	0.5	0.68	0.347	0.735	0.2	0.41
CD_0	0.102	0.042	0.08	0.024	0.263	0.055	0.05
CL_α	5.7	5.5	4.52	4.8	3.44	2	4.44
CD_α	0.66	0.47	0.27	0.15	0.45	0.38	0.33
Cm_α	-1.26	-1.6	-0.903	-0.65	-0.64	-1.3	-0.683
$CL_{\dot{\alpha}}$	6.7	0.006	2.7	2.7	0	0	0
$Cm_{\dot{\alpha}}$	-3.2	-9	-4.13	-4.5	-1.6	-2	-4.36
CL_q	5.4	6.58	7.72	7.5	0	0	3.8
Cm_q	-20.8	-25	-12.1	-4.5	-5.8	-4.8	-9.96
CL_{Mach}	-0.81	0.2	0	0	0	-0.2	0
CD_{Mach}	0	0.25	0	0	0	0	0
Cm_{Mach}	0.27	-0.1	0	0	0	-0.01	0
$CL_{\delta e}$	0.338	0.3	0.213	0.19	0.68	0.52	0.355
$Cm_{\delta e}$	-1.34	-1.2	-0.637	-0.57	-1.46	-0.1	-0.923
Lateral:							
CY_β	-0.96	-0.85	-0.877	-0.812	-1.17	-1	-0.564
Cl_β	-0.221	-0.1	-0.196	-0.177	-0.175	-0.09	-0.074
Cn_β	0.15	0.2	0.139	0.129	0.5	0.24	0.071
Cl_p	-0.45	-0.3	-0.381	-0.312	-0.285	-0.27	-0.41
Cn_p	-0.121	0.2	-0.049	-0.011	0.14	-0.09	-0.0575
$Cl_{\delta r}$	0.101	0.2	0.198	0.153	0.265	0.15	0.107
$Cn_{\delta r}$	-0.3	-0.325	-0.185	-0.165	-0.75	-0.65	-0.125
$Cl_{\delta a}$	0.0461	0.014	-0.038	-0.05	0.039	0.017	-0.134
$Cn_{\delta a}$	0.0064	0.003	0.017	0.008	0.0042	0.0025	-0.0035
$CY_{\delta r}$	0.175	0.075	0.216	0.184	0.208	0.05	0.157
$Cl_{\delta r}$	0.007	0.005	0.0226	0.019	0.045	0.008	0.107
$Cn_{\delta r}$	-0.109	-0.09	-0.096	-0.076	-0.16	-0.04	-0.072

Table C.2: Aircraft Stability Coefficients

Appendix D Development of State-space Matrix Parameters

The development of the state-space matrices for both the longitudinal and lateral dynamics is based on the parameters of Appendix C. Except where noted equations used throughout this appendix are stated in or derived from [2]. The notation employed here, for both the coefficients and derivatives, is based on partial derivatives.

$$CD_u = \frac{\partial(CD)}{\partial u}$$

"Derivative of Coefficient of Drag (*CD*) with respect to body forward velocity (*u*)"

D.1 Calculated Stability Derivatives

Several parameters listed in Appendix C are dependent on the nominal Mach number. Several equations are employed to convert the Mach number dependence to a body forward velocity (*u*) dependence.

$$CL_u = CL_{Mach}\left(\frac{Mach^2}{1 - Mach^2}\right)$$

$$CD_u = CD_{Mach} * Mach$$

$$Cm_u = Cm_{Mach} * Mach$$

Aerodynamic force coefficients, based on lift and drag, are converted to body force coefficients.

$$CX_u = -\left(CD_u + 2 * CD_0\right)$$

$$CX_w = -\left(CD_\alpha - CL_0\right)$$

$$CX_{\dot{\alpha}} = 0$$

$$CZ_u = -\left(CL_u + 2 * CL_0\right)$$

$$CZ_w = -\left(CL_\alpha + CD_0\right)$$

$$CZ_{\delta_e} = -CL_{\delta_e}$$

$$CY_{\delta_a} = 0$$

D.2 Assumed Stability Coefficients

Several assumption related to the body side force coefficient are required to complete the set of stability coefficients as provided in [2]. For this project the body right force (*Y*) was assumed to not be dependent upon either roll rate (*p*) or yaw rate (*r*).

$$CY_p = 0$$

$$CY_r = 0$$

D.3 Stability and Control Derivatives

In order to determine their actual force and moment dependence the non-dimensional stability and control coefficients are converted to stability and control derivatives. These are then incorporated directly into the state-space matrices.

D.4 Longitudinal Derivatives

$$X_u = CX_u * \left(\frac{Q * S}{m * u_0} \right)$$

$$X_w = CX_w * \left(\frac{Q * S}{m * u_0} \right)$$

$$X_{\delta_e} = CX_{\delta_e} * \left(\frac{Q * S}{m} \right)$$

$$Z_u = CZ_u * \left(\frac{Q * S}{m * u_0} \right)$$

$$Z_w = CZ_w * \left(\frac{Q * S}{m * u_0} \right)$$

$$Z_\alpha = Z_w * u_0$$

$$Z_{\delta_e} = CZ_{\delta_{ee}} * \left(\frac{Q * S}{m} \right)$$

$$M_u = Cm_u * \left(\frac{Q * S * c}{2 * m * u_0} \right)$$

$$M_w = Cm_\alpha * \left(\frac{Q * S * c}{I_y * u_0} \right)$$

$$M_{\dot{w}} = Cm_{\dot{\alpha}} * \left(\frac{Q * S * c^2}{2 * I_y * u_0{}^2} \right)$$

$$M_q = Cm_q * \left(\frac{Q * S * c^2}{2 * I_y * u_0} \right)$$

$$M_{\delta_e} = Cm_{\delta_e} * \left(\frac{Q * S * c}{I_y} \right)$$

D.5 Lateral Derivatives

$$Y_\beta = CY_\beta * \left(\frac{Q * S}{m} \right)$$

$$Y_p = CY_p * \left(\frac{Q * S * b}{2 * m * u_0} \right)$$

$$Y_r = CY_r * \left(\frac{Q * S * b}{2 * m * u_0} \right)$$

$$Y_{\delta_a} = CY_{\delta_a} * \left(\frac{Q * S}{m} \right)$$

$$Y_{\delta_r} = CY_{\delta_r} * \left(\frac{Q * S}{m} \right)$$

$$N_\beta = Cn_\beta * \left(\frac{Q * S * b}{I_z} \right)$$

$$N_p = Cn_p * \left(\frac{Q * S * b^2}{2 * I_z * u_0} \right)$$

$$N_r = Cn_r * \left(\frac{Q * S * b^2}{2 * I_z * u_0} \right)$$

$$N_{\delta_a} = Cn_{\delta_a} * \left(\frac{Q * S * b}{I_z} \right)$$

$$N_{\delta_r} = Cn_{\delta_r} * \left(\frac{Q * S * b}{I_z} \right)$$

$$L_\beta = Cl_\beta * \left(\frac{Q * S * b}{I_x} \right)$$

$$L_p = Cl_p * \left(\frac{Q * S * b^2}{2 * I_x * u_0} \right)$$

$$L_r = Cl_r * \left(\frac{Q * S * b^2}{2 * I_x * u_0} \right)$$

$$L_{\delta_a} = Cl_{\delta_a} * \left(\frac{Q * S * b}{I_x} \right)$$

$$L_{\delta_r} = Cl_{\delta_r} * \left(\frac{Q * S * b}{I_x} \right)$$

D.6 State space matrices

$$A_{longitudinal} = \begin{bmatrix} X_u & X_w & 0 & -g \\ Z_u & Z_w & u_o & 0 \\ M_u + M_{\dot{w}} Z_u & M_w + M_{\dot{w}} Z_w & M_q + M_{\dot{w}} u_o & 0 \\ 0 & 0 & 1 & 0 \end{bmatrix}$$

$$B_{longitudinal} = \begin{bmatrix} X_{\delta_e} & X_{\delta_T} \\ Z_{\delta_e} & Z_{\delta_T} \\ M_{\delta_e} + M_{\dot{w}} Z_{\delta_e} & M_{\delta_T} + M_{\dot{w}} Z_{\delta_T} \\ 0 & 0 \end{bmatrix}$$

$$A_{lateral} = \begin{bmatrix} \frac{Y_\beta}{u_o} & \frac{Y_p}{u_o} & \frac{Y_r}{u_o} - 1 & \frac{g\cos(\theta_o)}{u_o} \\ L_\beta & L_p & L_r & 0 \\ N_\beta & N_p & N_r & 0 \\ 0 & 1 & 0 & 0 \end{bmatrix}$$

$$B_{lateral} = \begin{bmatrix} \frac{Y_{\delta_a}}{u_o} & \frac{Y_{\delta_r}}{u_o} \\ L_{\delta_a} & L_{\delta_r} \\ N_{\delta_a} & N_{\delta_r} \\ 0 & 0 \end{bmatrix}$$

Bibliography

[1] Bernard Etkin. Dynamics of Flight - Stability and Control. John Wiley and Sons, second edition, 1982.

[2] Robert C. Nelson. Flight Stability and Automatic Control. McGraw-Hill, 1989.

[3] Haim Baruh. Analytical Dynamics. McGraw-Hill, 1999.

[4] Jacob Reiner, Gary J. Balas and William L. Garrard. "Flight Control Design Using Robust Dynamic Inversion and Time-scale Separation." Automatica, 32(11):1493-1504, 1996.

[5] Hakan Fer and Dale F. Enns. "An Approach to Select Desired Dynamics Gains for Dynamic Inversion Control Laws." AIAA Guidance, Navigation, and Control Conference, New Orleans, LA, Aug. 11-13, 1997, Collection of Technical Papers.

[6] John Kaneshige, John Bull and Joseph J. Totah. "Generic Neural Flight Control and Autopilot System." AIAA Guidance, Navigation, and Control Conference and Exhibit, Denver, CO, Aug. 14-17, 2000.

[7] Systems Planning and Analysis, Inc. "For Use with MATLAB Mapping Toolbox." The Mathworks, Inc, 2002.